NMR Structure and Dynamics of the Second Transmembrane Domain of the Neuronal Acetylcholine Receptor β 2 Subunit †

ARTICLE *in* BIOCHEMISTRY · DECEMBER 2003

Impact Factor: 3.02 · DOI: 10.1021/bi0350396 · Source: PubMed

3 AUTHORS, INCLUDING:

Victor E. Yushmanov
University of Pittsburgh
97 PUBLICATIONS **818** CITATIONS
SEE PROFILE

Pei Tang
University of Pittsburgh
142 PUBLICATIONS **2,194** CITATIONS
SEE PROFILE

NMR Structure and Dynamics of the Second Transmembrane Domain of the Neuronal Acetylcholine Receptor β_2 Subunit†

Victor E. Yushmanov,‡ Yan Xu,‡,§ and Pei Tang*,‡,§

Department of Anesthesiology and Department of Pharmacology, University of Pittsburgh School of Medicine, Pittsburgh, Pennsylvania 15261

Received June 17, 2003; Revised Manuscript Received September 15, 2003

ABSTRACT: Structure and backbone dynamics of a selectively [^{15}N]Leu-labeled 28-residue segment of the extended second transmembrane domain (TM2e) of the human neuronal nicotinic acetylcholine receptor (nAChR) β_2 subunit were studied by ^{1}H and ^{15}N solution-state NMR in dodecylphosphocholine micelles. The TM2e structure was determined on the basis of the nuclear Overhauser effects (NOEs) and the hydrogen bond restraints, which were inferred from the presence of $H^{\alpha}_i-H^{N}_{i+3}$, $H^{\alpha}_i-H^{\beta}_{i+3}$, and $H^{\alpha}_i-H^{N}_{i+4}$ NOE connectivity and from the slow amide hydrogen exchange with D_2O. The TM2e structure of the nAChR β_2 subunit contains a helical region between T4 and K22. Backbone dynamics were calculated using the model-free approach based on the ^{15}N relaxation rate constants, R_1 and R_2, and on the $^{15}N-\{^1H\}$ NOE. The data acquired at 9.4 and 14.1 T and calculations using different dynamic models demonstrated no conformational exchange and internal motions on the nanosecond time scale. The global tumbling time of TM2e in micelles was 14.4 ± 0.2 ns; the NOE values were greater than 0.63 at 9.4 T, and the order parameter, S^2, was 0.83−0.96 for all ^{15}N-labeled leucine residues, suggesting a restricted internal motion. This is the first report of NMR structure and backbone dynamics of the second transmembrane domain of the human nAChR β_2 subunit in a membrane-mimetic environment, providing the basis for subsequent studies of subunit interactions in the transmembrane domain complex of the neuronal nAChR.

The nicotinic acetylcholine receptor (nAChR)[1] is one of the most extensively studied members of a superfamily of neurotransmitter-gated ion channels (*1*, *2*) that are responsible for the fast synaptic transmission in the central and peripheral nervous systems. It is believed that each receptor is composed of five subunits and that each subunit consists of an extended extracellular N-terminus, four transmembrane domains (TM1−TM4), and a short C-terminus. On the basis of the studies of photoaffinity labeling, substituted cysteine accessibility, mutagenesis, and electrophysiology analyses, it was suggested that the TM2 domains of five subunits line the pore of the channel (*2*, *3*). The electron microscopic image of a whole *Torpedo* nAChR channel was obtained at a resolution of 4−9 Å (*4*, *5*). Recently, the crystal structure of the molluscan acetylcholine-binding protein has reached a resolution of 2.7 Å (*6*). Because of the homology of its sequence to those of the N-terminal domains of the nAChR subunits, this very high resolution structure provides a good structural template for the extracellular domain of nAChRs. High-resolution structures of transmembrane domains of nAChRs, however, are still elusive. To achieve atomic resolution for the structures of transmembrane domains, one of the feasible approaches is to determine the structure of one or two domains at a time by high-resolution nuclear magnetic resonance (NMR) spectroscopy (*7*). Using this approach, we have recently obtained TM2 structures of the human glycine receptor (GlyR) α_1 subunit in membrane-mimetic dodecylphosphocholine (DPC) and sodium dodecyl sulfate (SDS) micelles (*8*, *9*).

The nAChRs comprise a large number of subtypes with different combinations of various subunits. Most of the studies related to nAChRs so far have been focused on the muscle-type receptors derived either from the skeletal muscle or from the *Torpedo* electric organ. This is mainly due to the relatively widespread availability of this type of nAChR. Isolated transmembrane domains TM2 and TM3 of the *Torpedo* nAChR α_1 subunit in a chloroform/methanol mixture (*10*, *11*) and TM2 of the muscle-type δ subunit in DPC micelles and lipid bilayers (*7*, *12*) have been characterized by NMR. The detailed structural data for transmembrane domains of neuronal nAChRs, however, are currently unavailable. Although it is reasonable to assume that domain structures of muscular and neuronal nAChRs are similar because of their sequence homology, resolving the subtle structural difference between subtypes may lead to a better

† This work was supported by NIH Grant R01 GM56257 to P.T.

* To whom correspondence should be addressed: W1357 Biomedical Science Tower, University of Pittsburgh, Pittsburgh, PA 15261. Telephone: (412)383-9798. Fax: (412)648-9587. E-mail: tangp@anes.upmc.edu.

‡ Department of Anesthesiology.

§ Department of Pharmacology.

[1] Abbreviations: nAChR, nicotinic acetylcholine receptor; NMR, nuclear magnetic resonance; DPC, dodecylphosphocholine; SDS, sodium dodecyl sulfate; R_1 and R_2, longitudinal and transverse relaxation rate constants, respectively; NOE, nuclear Overhauser effect; GlyR, glycine receptor; CD, circular dichroism; TM2e, extended TM2 segment of the human neuronal nAChR β_2 subunit; 2D, two-dimensional; 5-DSA, 5-DOXYL-stearic acid; DMPC, dimyristoylphosphatidylcholine; NOESY, NOE spectroscopy; TOCSY, total correlation spectroscopy; HSQC, heteronuclear single-quantum coherence; τ_m, global rotational correlation time; S^2, squared order parameter; R_{ex}, exchange rate constant; τ_e, effective correlation time for fast internal motions; TM1−TM4, transmembrane domains 1−4, respectively.

10.1021/bi0350396 CCC: $25.00
Published on Web 10/18/2003

understanding of the difference in their biochemical and physiological functions.

The neuronal nAChRs consist of only two types of subunits (*13*): an α-type or agonist binding subunit and a *β*-type or structural subunit. The naming of the α-type neuronal nAChR subunits is based on their substantial homology with the α subunit of the muscle nAChR, including the presence of vicinal cysteine residues (Cys192 and Cys193; α1 numbering) as a flag for the ACh-binding site of muscle-type nAChRs. The muscle α subunit is denoted as α1, and α2−α10 are distinct neuronal α subunits (*13*, *14*). Three members of the neuronal nAChR *β*-type subunit group, *β*2−*β*4, have to date been identified. Unlike the α subunit, the neuronal *β* subunits lack equivalents of Cys192 and Cys193 and are not highly homologous with the muscle *β* subunit.

Among all neuronal nAChRs, $2\alpha_4 3\beta_2$ is a predominant subtype of nAChRs in the central nervous system. The presence of the β_2 subunit seems to be required for the anatomical and functional development of the visual system (*15*) and for the protective responses to stress (*16*). Overexpression and certain mutations of the β_2 subunit have been associated with the development of Down syndrome (*17*) and nocturnal frontal lobe epilepsy (*18*). It has also been shown that neuronal heteromeric nAChRs containing β_2 subunits are particularly sensitive to volatile general anesthetics (*19*−*21*). Site-directed mutagenesis within the TM2 domain has identified a specific amino acid as being critical for the sensitivity of the nAChR to anesthetics (*21*, *22*). High-resolution domain structures of the β_2 subunits seem to be essential for gaining insights into the molecular details of these mutation-induced functional changes.

It has been generally realized that protein motions are important determinants of the stability and function of proteins (*23*). Our recent results suggest that low-affinity drugs, such as volatile general anesthetics, may exert their action by altering protein dynamics instead of changing protein structures (*24*, *25*). The theory and techniques for determining protein dynamics using solution NMR have been well developed (*23*, *26*). Overall protein backbone dynamics are often probed by the motions of backbone N−H vectors and detected through parameters that are sensitive to the strength of $^{15}N-^{1}H$ dipolar interactions and ^{15}N chemical shift anisotropy, including the longitudinal and transverse relaxation rate constants (R_1 and R_2, respectively) and the $^{15}N-\{^{1}H\}$ steady-state nuclear Overhauser effect (NOE) of an amide ^{15}N. We have previously determined the structure and backbone dynamics of the TM2 domain of the human GlyR α_1 subunit in SDS and DPC micelles using high-resolution NMR (*8*, *9*). We found restricted internal motions in the helical region and a relatively high degree of motional freedom of the TM2 domain of the GlyR α_1 subunit in micelles. The dynamics of the nAChR, however, have not been studied previously.

Reconstitution of membrane-associated proteins and peptides into micelles of surfactants, such as DPC, is a common approach to determining their structure and dynamics using high-resolution solution-state NMR techniques. The channel-lining TM2 segments of the muscle nAChR and of the NMDA receptor were studied in DPC micelles and lipid bilayers by solution and solid-state NMR (*7*). It was shown that, when reconstituted in bilayers, the TM2 segments of the nAChR *δ* subunit and of the neuronal nAChR α_4 subunit alone form homopentameric channels with conductance characteristics very similar to those of a natural receptor (*7*). It has also been demonstrated recently that pentameric bundles of TM2 segments of the GlyR could form in micelles (*8*), suggesting that micelles may provide an adequate membrane-mimicking environment for transmembrane channel assembly. Hence, the study of isolated functional segments of the TM2 domains of nAChR in micelles is warranted.

In this work, we report structure and backbone dynamics of a peptide segment corresponding to the extended TM2 chain of the human neuronal nAChR β_2 subunit (TM2e) using solution-state NMR spectroscopy in DPC micelles. TM2e contains the putative transmembrane segment TM2 and seven residues at the C-terminus that belong to the linker region between TM2 and TM3. Seven leucine residues in TM2e, widely spread along the segment, were selectively labeled with ^{15}N for the ^{15}N NMR measurements of backbone dynamics. The TM2e orientation within membrane bilayers was probed by solid-state NMR spectroscopy.

MATERIALS AND METHODS

Sample Preparation. The selectively [^{15}N]Leu-labeled, extended TM2 domain of the human neuronal nAChR β_2 subunit, TM2e (EKMTLCISVLLALTVFLLLISKIVPPTS, molecular mass of 3.05 kDa), was obtained by solid-phase synthesis. For reconstitution of the TM2e peptide into DPC micelles, a solution of 4.6−7.7 mg of TM2e in trifluoroethanol was dried into a thin film under a stream of nitrogen gas. An aqueous solution of DPC (Avanti Polar Lipids, Alabaster, AL) was added to reach a DPC/peptide molar ratio of 150. After being vigorously mixed, the sample was lyophilized and rehydrated to final peptide and DPC concentrations of 3 and 450 mM, respectively, with 250 mM NaCl at pH 5 in water containing 10% D_2O for deuterium lock in the NMR measurements. For homonuclear two-dimensional (2D) ^{1}H NMR, perdeuterated DPC-d_{38} and a final peptide concentration of 5 mM was used. DPC-d_{38} and D_2O were obtained from Cambridge Isotope Laboratories (Andover, MA). To introduce the lipid nitroxyl spin probe 5-DOXYL-stearic acid (5-DSA, from Aldrich, Milwaukee, WI) into the micelles, an aliquot of a 5-DSA solution in ethanol was evaporated under nitrogen gas before mixing it with TM2e in DPC. The maximum concentration of 5-DSA reached 7.8 mM, i.e., approximately one 5-DSA molecule per micelle.

For the samples of TM2e in aligned phospholipid bilayers (*7*, *27*), 7 mg of TM2e, 64 mg of dimyristoylphosphatidylcholine (DMPC), and 8 mg of DMPC-d_{54} (Avanti Polar Lipids) were dissolved in trifluoroethanol, mixed, sonicated for 5 min, and stored overnight at −20 °C. This solution (with a DMPC:peptide molar ratio of approximately 45) was evenly distributed over 52 glass slides (5.7 mm × 12 mm each), air-dried, and vacuum-dried overnight. MilliQ water was added to each slide (3 *μ*L per slide); the slides were stacked into a parallelepiped glass tube, and equilibrated in a chamber with a saturated solution of ammonium phosphate at 37 °C for at least 15 h. When the desirable degree of sample hydration and alignment was achieved (as monitored by ^{2}H and ^{31}P NMR), the glass tube was sealed.

CD Spectroscopy. CD spectra in the wavelength range from 185 to 290 nm were obtained at 25 °C on an Aviv CD spectrometer (model 202, Aviv Instruments, Lakewood, NJ) with a 1 mm cuvette using a wavelength step of 1 nm and averaging time of 1 s, and analyzed using the Web-based CD analysis software DICHROWEB at www.cryst.bbk.ac.uk/cdweb/html/home.html (*28*).

NMR Spectroscopy. Solution NMR spectra were recorded at 30 °C on a Bruker Avance-600 NMR spectrometer (Bruker Instruments, Billerica, MA) equipped with a triple-resonance, triple-axis gradient TBI probe, and a Chemagnetics CMX-400SLI spectrometer (Varian NMR, Inc., Fort Collins, CO) equipped with a Z-gradient broadband Z-SPEC probe (Nalorac Cryogenics Corp., Martinez, CA). Operating frequencies were 600.83 and 401.10 MHz, respectively, for ^{1}H and 60.88 and 40.64 MHz, respectively, for ^{15}N. ^{15}N-decoupled ^{1}H homonuclear 2D NOE spectroscopy (NOESY) and total correlation spectroscopy (TOCSY) data were typically acquired at 600 MHz as 2048 t_2 and 640 t_1 data points with a spectral width of 10 ppm in each dimension, with 72−80 transients per increment. TOCSY and NOESY mixing times were 60 and 100−150 ms, respectively. All spectra were obtained in the phase-sensitive (States−TPPI) mode. For suppression of the solvent peak, the WATERGATE pulse scheme was applied. Gradient-selected, sensitivity-enhanced ^{1}H−^{15}N heteronuclear single-quantum correlation (HSQC) data were typically acquired as 2048 t_2 and 80 t_1 data points, with a spectral width of 12−14 ppm for ^{1}H and 25 ppm for ^{15}N. To assess the rates of exchange of amide protons, a series of HSQC spectra was acquired 20 min after rehydration of the lyophilized sample with D_2O. In 20 h, a NOESY spectrum was acquired to observe the amide protons having very slow ^{1}H−^{2}D exchange rates. Spin−lattice (R_1) and spin−spin (R_2) ^{15}N relaxation rate constants and ^{15}N−{^{1}H} NOE values were repeatedly measured for each of the ^{15}N amides using standard pulse sequences with Echo−Antiecho gradient selection (*29*). In relaxation measurements, 80 t_1 data points were used with intervals of 1.5 s between scans, and nine variable delays ranging from 20 to 1200 ms at 401 MHz or 1500 ms at 600 MHz for R_1, and between 17 and 160 ms for R_2. In NOE experiments, 80 indirect data points were acquired with or without proton saturation in an interleaved fashion. Saturation was achieved by a train of 120° pulses at 5 ms intervals for 3 s.

Solid-state ^{15}N NMR spectra were obtained at 40.6 MHz on a 89 mm bore Oxford magnet interfaced with a Bruker console at 30 °C using cross polarization with a contact time of 1 ms and a recycle delay of 7 s (*27*). Glass slides were positioned in the magnet with the glass plate normal parallel to the direction of the static magnetic field. ^{15}N chemical shifts were referenced to $^{15}NH_4NO_3$ at 0 ppm. To monitor phospholipid alignment, solid-state ^{2}H and ^{31}P spectra of the same samples were recorded at 35 °C on a Chemagnetics CMX-400SLI spectrometer at 61.6 and 162.4 MHz, respectively.

Data Processing and Analysis. Data were processed using NMRPipe 4.1 and NMRDraw 1.8 (*30*), and analyzed using PIPP (*31*) and Sparky 3.100 (*32*) software. For structure calculations, distance restraints, derived from NOESY experiments, were classified into four groups, i.e., <2.9, <3.5, <5.0, and <6.0 Å for strong, medium, weak, and very weak NOEs, respectively (*33*). For residues involved in hydrogen bonding, hydrogen bonds between CO(i) and NH(i+4) were included as constraints by restraining r_{NH-O} to 1.2−1.9 Å and r_{N-O} to 1.8−2.9 Å (*34*, *35*). Assessment of hydrogen bonding was carried out on the basis of the presence of $d_{\alpha N}$(i,i+3), $d_{\alpha\beta}$(i,i+3), and $d_{\alpha N}$(i,i+4) NOE connectivity, and on the basis of the exchange rates for the amide protons (*7*). The initial structure calculations were performed iteratively using NOE constraints with the simulated annealing protocol (*36*) in X-PLOR-NIH 2.02 (*37*, *38*). Lowest-energy structures with no violations above the threshold conditions of 5° for angle, improper, and dihedral angles and 0.05 and 0.5 Å for bonds and NOEs, respectively, were taken for further refinement. For the final round of calculations, 100 structures were calculated and refined. In dynamic studies, ^{15}N R_1 and R_2 values were determined from two-parameter fits of peak intensities versus variable delay to single-exponential functions. ^{15}N−{^{1}H} NOE values are reported as peak intensity ratios obtained with and without ^{1}H saturation. The global tumbling time (τ_m) was initially estimated from the R_2/R_1 ratio (*39*). Determination of the rotational diffusion tensor was performed using Tensor 2.0 (*40*). The squared order parameter (S^2), the exchange rate constant (R_{ex}), the effective correlation time for fast internal motions (τ_e), and the refined τ_m value were obtained by fitting the experimentally measured R_1, R_2, and NOE values in the framework of Lipari−Szabo formalism (*41*, *42*) and subsequent Monte Carlo numerical simulations using the Modelfree 4.15 software package (*43*, *44*).

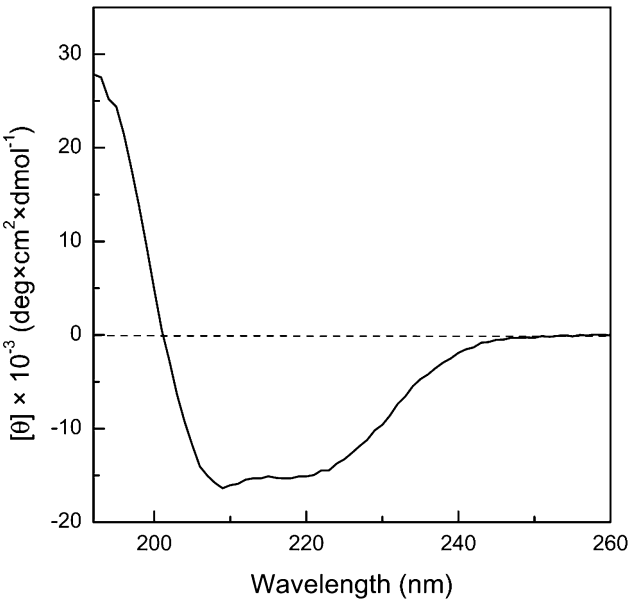

FIGURE 1: Far-UV CD spectrum of the TM2e peptide of the human *n*-acetylcholine receptor β_2 subunit in aqueous micelles of DPC at 25 °C.

RESULTS

Structure of TM2e. In DPC micelles, CD and NMR spectra of TM2e showed the presence of helical secondary structure. Figure 1 depicts a representative CD spectrum. Analysis using the CDSSTR and K2D methods in the Web-based DICHROWEB package yielded 49 and 59% of the α-helical component, respectively. Homonuclear 2D TOCSY, NOESY, and ^{1}H−^{15}N HSQC experiments allowed for the ^{1}H peak assignment for most of the TM2e residues in DPC and the

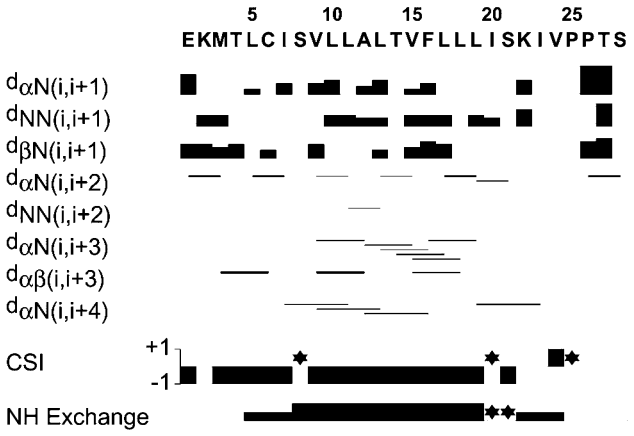

FIGURE 2: Summary of sequential and midrange NOE connectivity (mixing time of 150 ms) and the chemical shift index (CSI) in the TM2e peptide of the human *n*-acetylcholine receptor β_2 subunit in DPC micelles. The widths of the lines are related to the observed NOE intensities. The connectivity is not reported when cross-peaks were below the noise level, or overlapped with diagonal (in the case of sequential $H^N_i-H^N_{i+1}$ NOEs) or other cross-peaks. For CSI, stars denote the residues whose H^α peaks are indistinguishable in the spectra. For amide exchange, the thick, intermediate, and thin strips represent the amide protons whose cross-peaks were unchanged, decreased, and not detectable, respectively, in the NOESY spectrum started 20 h after rehydration of the lyophilized sample with D_2O. Stars indicate that the degree of the decrease in the magnitude of the signal was unclear because of the low signal-to-noise ratio for the corresponding peaks in the spectra of nonexchanged TM2e.

^{15}N peak assignments for seven leucine residues (see the resonance assignment table in the Supporting Information). As is often the case for peptides in micelles, NMR lines experience considerable broadening, resulting in overlapping or missing peaks for a few residues, especially in TOCSY spectra. Nevertheless, more than 300 NOE cross-peaks were identified and assigned. Figure 2 summarizes the NOE connectivity, the chemical shift indices, and the classification of the backbone amide proton exchange rate. Midrange $H^\alpha_i-H^N_{i+3}$, $H^\alpha_i-H^\beta_{i+3}$, and $H^\alpha_i-H^N_{i+4}$ connectivity was found from residue M3 to I23, indicating an α-helical structure in this region. The secondary chemical shift index, determined on the basis of H^α proton chemical shifts from the corresponding random coil values (*45*), also provided a preliminary identification of the helical structure approximately between the N-terminus and residue I23. ^1H NMR spectra demonstrate the high structural stability of TM2e in DPC: only E1, K2, and T4 exhibited changes in their chemical shifts after the sample was kept at room temperature for several weeks.

Amide hydrogen exchange of TM2e in DPC was monitored by NOESY for all residues and by HSQC for leucine residues. A representative HSQC spectrum of TM2e is shown in Figure 3. As presented in Figure 2, amide protons of the residues in either the N- or C-terminus have a relatively high exchange rate: their peaks disappeared in the NOESY spectrum 20 h after the sample was rehydrated in D_2O. During the same time period, peak intensities of the residues close to both termini, such as L5−I7 and I20−V24, were reduced significantly because of slow $^1H-^2D$ exchange, while those of the residues between S8 and L19 were unaltered, showing a high degree of protection from exchange. The pattern of $^1H-^2D$ exchange along the sequence

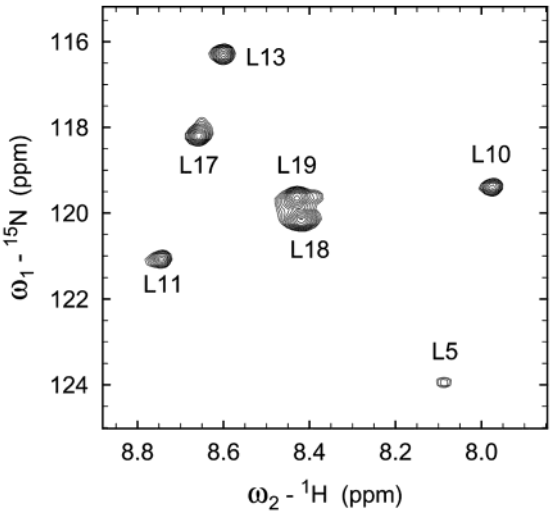

FIGURE 3: Amide backbone region of a $^1H-^{15}N$ HSQC NMR spectrum of 3.0 mM TM2e of the human *n*-acetylcholine receptor β_2 subunit in aqueous DPC micelles at 30 °C and at a ^1H resonance frequency of 600.83 MHz.

revealed a structure profile of TM2e and provided useful hydrogen bonding constraints for the structure refinement.

Twenty lowest-energy structures that satisfy the NMR data without violations within the specified limits (see Materials and Methods) are shown in Figure 4. They adopt a helical structure between T4 and K22, with an rmsd of 0.13 ± 0.05 Å for the backbone and 0.90 ± 0.26 Å for all heavy atoms in this region. Although the helix extension is slightly longer than the region with very slow amide exchange (S8−L19), it is in line with the midrange connectivity and the secondary chemical shift index. Within the precision of experimental procedures, the helical fraction in NMR structures is consistent with that estimated from the CD spectra. Residues T4, S8, L11, V15, and L19 form a well-defined path along the side of TM2e. The structure is consistent with the results obtained by other methods, indicating that these residues face the pore lumen of an assembled pentameric nAChR channel (*2*, *5*).

Backbone Dynamics of TM2e. The backbone dynamics of TM2e were determined by ^{15}N relaxation of seven selectively ^{15}N-labeled Leu residues. As summarized in Figure 5, all Leu residues have similar motional characteristics. Relatively high NOE values (>0.6 at 401 MHz and >0.7 at 600 MHz) indicate that all leucines are located in the regions with restricted internal motions. At higher magnetic fields, spin−lattice relaxation (R_1 constant) was much slower and the NOE tended to increase, as expected from the theory, whereas spin−spin relaxation (R_2 constant) did not change appreciably with the magnetic field. The R_2/R_1 ratio for those residues whose relaxation is not affected by the fast internal motions on the picosecond time scale is virtually independent of the internal motion and provides an initial estimation for the reorientation time of each NH vector with global tumbling, i.e., the τ_m of the peptide (*39*). Initial estimates of the τ_m value of TM2e in DPC obtained from the R_2/R_1 ratio and averaged over all seven leucine residues yielded a value of 14.4 ns at 401 MHz and 15.2 ns at 600 MHz. A slightly higher τ_m value at higher frequencies might be due to possible contributions of the exchange term (R_{ex}) to R_2 (*46*). There-

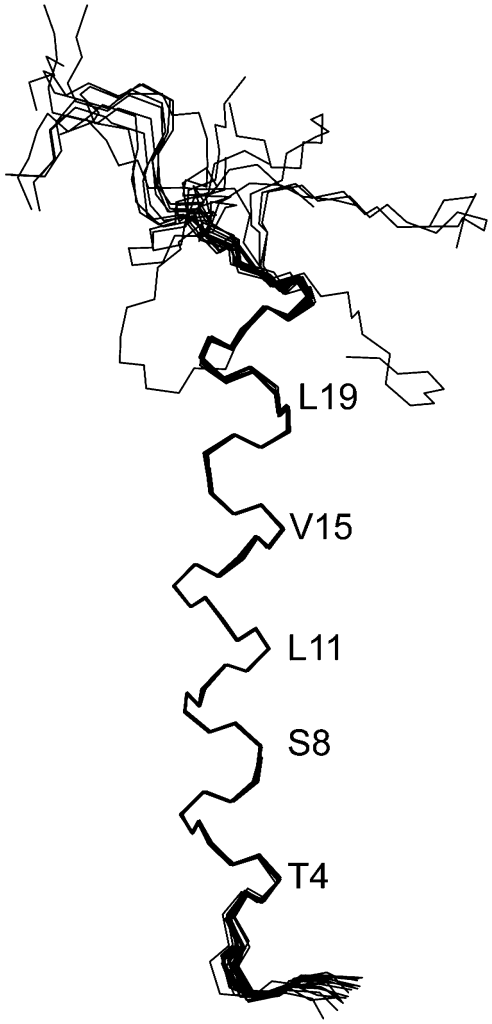

FIGURE 4: Structures calculated from restraints derived from NMR experiments for TM2e in DPC micelles. Backbone traces of the 20 lowest-energy structures are presented with the C-terminus pointing up.

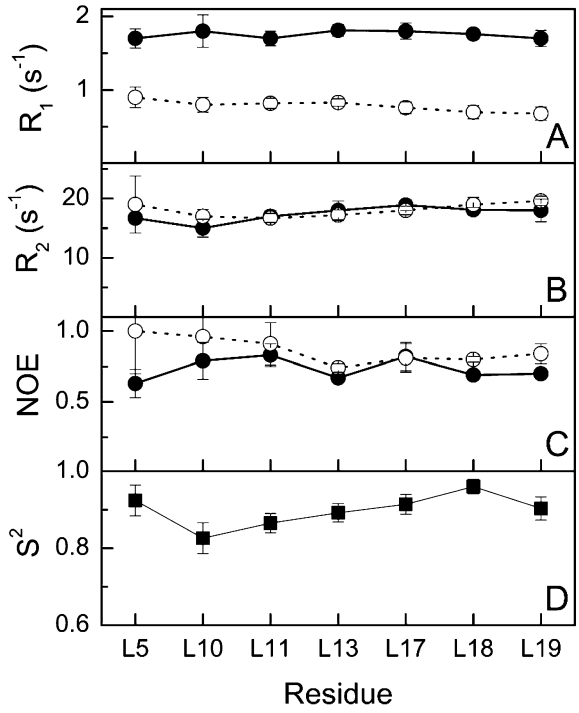

FIGURE 5: Relaxation rate constants R_1 (A) and R_2 (B), $^{15}N-\{^1H\}$ NOE values (C), and squared order parameter S^2 (D) for leucine amides of TM2e in DPC micelles at 30 °C. Relaxation data in panels A−C were obtained at 401 MHz (●) and 600 MHz (○). For 401 MHz measurements, all data represent average values over three to four experiments. Errors were derived from the statistical dispersion and either from the uncertainties of the least-squares fit to the exponential decay function (for R_1 and R_2) or from the signal-to-noise ratios (for NOE). For S^2 (D), error bars are standard deviations derived from 300 Monte Carlo simulations.

fore, attention has been paid to careful selection of a dynamical model, as described below.

Using our structural data and ^{15}N relaxation data as input, the parameters of the molecular rotational diffusion tensor were calculated (*40*), proving the isotropic diffusion for TM2e in DPC. An appropriate dynamical model for each given spin was then selected, as described previously (*44*). To assess the fit of any single model to the relaxation data, confidence limits were estimated on the basis of 300 Monte Carlo simulations. It was found that most of the relaxation data fit best to the dynamical model with only one model-free parameter, S^2. In several cases when alternative models were also considered (for L13, L17, and L18), the exchange contribution to R_2 was relatively insignificant (comparable to the error in R_2), and the τ_e values were in agreement with fast local motions (tens to hundreds of picoseconds). At the last stage of calculations, the τ_m value was optimized simultaneously with appropriate dynamics parameters (S^2, R_{ex}, and τ_e) for the backbone N−H bonds of each leucine residue. The optimized τ_m value of TM2e in DPC was 14.4 ± 0.2 ns. This value is very close to those estimated from the R_2/R_1 ratio, thus suggesting the absence of significant contributions of exchange and slow internal motions, and validating the choice of the simple dynamical model. The results of model-free calculations are given in Figure 5D. It can be seen that for all leucine amides, the order parameter S^2 was between 0.83 and 0.96, showing restricted internal motions characteristic of well-defined secondary structure elements.

TM2e in Membrane-Mimetic Environments. The location of TM2e in the micelle was approached using hydrophobic spin probe 5-DSA, which induces the distance-dependent NMR line broadening of the nearby nuclei predominantly due to enhanced relaxation caused by the unpaired electron of the nitroxide radical. Although the specificity of DSA in highly dynamic ionic micelles is notoriously low (*47*), it is known from ^{13}C line width and ^1H T_1 measurements that the nitroxide radical of 5-DSA is distributed preferentially in the hydrophobic interior just underneath the polar headgroup (*48*−*51*). In particular, the density of the paramagnetic fragment of 5-DSA is highest at the hydrophobic side of the DPC phosphate groups (*51*, *52*). In our experiments, we monitored the paramagnetic effects of 5-DSA by the line broadening of lipid peaks in ^1H spectra of micelles, and by the intensity decrease of amide peaks in HSQC spectra. Although signals of the protons close to the headgroup were affected more than the signals from the hydrophobic micelle core (data not shown), 5-DSA broadened all DPC signals to some extent, which is similar to the observations in other micelles such as SDS (*47*). In the presence of 5-DSA, amide peak intensities of all leucine residues decreased in a concentration-dependent fashion. The peaks of L5 and L10

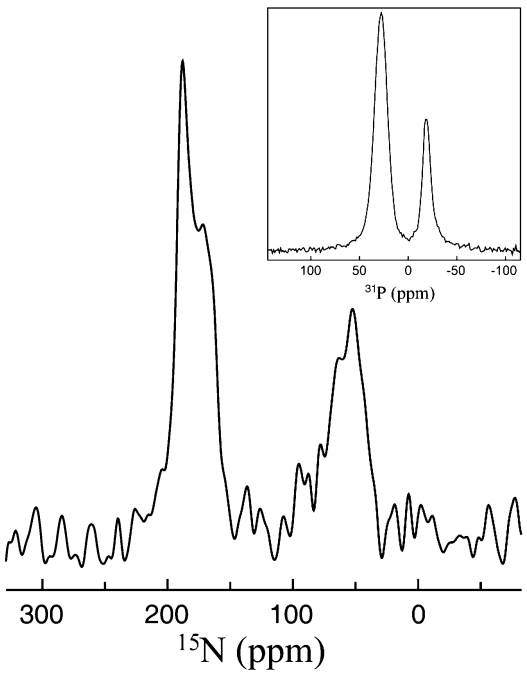

FIGURE 6: Solid-state ^{15}N NMR spectrum of TM2e in oriented bilayers of DMPC. The approximate DMPC:peptide molar ratio is 45. The inset shows a ^{31}P NMR spectrum of the same sample (^{31}P chemical shifts are referenced to the position of the isotropic peak at 0 ppm).

were affected the most, suggesting that these residues are located in the hydrophobic interior of the micelle close to the polar micelle−water interface. Five other leucine residues (in positions 11, 13, and 17−19) also experienced the effect of the spin probe, because the highly dynamic nature of micelles allows 5-DSA to penetrate deeper inside the micelle.

The TM2e orientation within the bilayer membrane was tested by solid-state ^{15}N NMR in oriented DMPC samples. Figure 6 demonstrates that the majority of the signals of the ^{15}N-labeled leucine are observed near 200 ppm, which is characteristic of a parallel orientation of the amide NH bond to the magnetic field. For an α-helix, this is generally taken to be an indication of the transmembrane orientation of the peptide (*7*, *27*). The rest of the TM2e signal at ∼50 ppm originates from the peptide partitioned in a nonoriented fraction of the lipid matrix. This is evidenced by the ^{31}P spectrum of the same sample showing a nearly identical ratio of the peaks of well-aligned (27 ppm) and nonaligned (−13 ppm) phospholipids (inset of Figure 6). We were unable to completely eliminate the nonoriented material, a common situation in this type of experiment. Its presence, however, does not detract from the conclusion about the orientation of TM2e in the bilayer.

DISCUSSION

This study determined the secondary structure of TM2e of the neuronal nAChR β_2 subunit in DPC micelles. An α-helical structure of TM2e between T4 and K22 spans the putative TM2 segment of nAChR (Figure 4). There is no well-defined secondary structure for the C-terminus, which is formed by part of the hinge region linking TM2 and TM3. The presence of a helical structure in the N-terminal region was indicated by the secondary chemical shifts and the $d_{\alpha\beta}(i,i+3)$ connectivity pattern (Figure 2), but the structure appears to be less stable, as evidenced by rapid amide hydrogen exchange and different conformational variation at E1, K2, and T4 several weeks after the rehydration of the sample. With the current experimental protocol, the oligomerization state of TM2e in DPC is predominantly monomeric with a relatively minor contribution of the oligomeric species. Therefore, the structure presented in Figure 4 is a weighted average of the monomer and a minor fraction of symmetric homooligomeric states.

Our structural data compare well with available NMR data on single transmembrane domains in related neurotransmitter-gated receptors. The ^{1}H NMR structure for TM2 of the *Torpedo* nAChR α_1 subunit in a chloroform/methanol mixture (*11*) was reported to adopt a right-handed α-helical secondary structure. A helix was defined in the region of the α_1 subunit homologous to the E1−I23 region in our TM2e of the neuronal β_2 subunit (*11*). In a study of TM2 of the *Torpedo* nAChR δ subunit in DPC micelles (*12*), the reported homonuclear ^{1}H NOE, the chemical shift index, and the amide hydrogen exchange data were very similar to those of β_2 TM2e in this study.

Earlier studies of the *Torpedo* nAChR suggested a kink at a highly conserved leucine residue of TM2 (*4*). In a more recent NMR study of the nAChR α_1 subunit, the helix distortion was suggested near L251 on the basis of the 0.5 ppm downfield amide ^{1}H shift of the leucine from the rest of the NH proton signals (*11*). In the latter work, it was proposed that the distortion of the TM2 helix in the α_1 subunit is caused by the competition of the side chain hydroxyls of S252 and T254 with backbone NH hydrogens for the backbone carbonyls, resulting in the T254 OH···OC L250 and S252 OH···OC S248 transient hydrogen bonds, and the lack of the S248 CO···HN S252 hydrogen bond (*11*). The L251 residue of the α_1 subunit, where the distortion was observed, is homologous to L249 in the β_2 subunit (*21*) and corresponds to L11 in TM2e. In our study, however, no evidence for the helix distortion was observed. Our data, including NOE connectivity, chemical shift index, and amide ^{1}H−^{2}D exchange pattern, revealed a stable helical structure in the region around L11. No distinct difference in the amide ^{1}H shift was found between L11 and the rest of the leucines (Figure 3). There was no evidence of kinks for TM2 of the muscle nAChR δ subunit in DPC either (*7*). The discrepancy between the presence of significant helix distortions in the α_1 subunit and their absence in the β_2 and δ subunits may exist for a variety of reasons. First, the β_2 subunit has alanine in position 12 which is homologous to S252 in the α_1 subunit, and the δ subunit has A12 and A14 where the α_1 subunit has S252 and T254, respectively (*7*, *12*). The critical difference between alanine and serine or threonine is that the side chain of alanine cannot be involved in hydrogen bonding. Therefore, the possibility of a helix distortion due to the competition of hydrogen bonding from side chains does not exist in that region of the β_2 and δ subunits. Second, the amide deuterium exchange data were not used as constraints for structure calculations of α_1 TM2 in organic solvent; rather, hydrogen bonds were assessed from analysis of calculated structures, thus complementing amide exchange data (*11*). Nevertheless, the pattern of hydrogen bonding may differ between micelles and organic solvent. The possibility of the "kink" due to cumulative small deviations of the peptide backbone from a perfect α-helical geometry, rather

than a marked distortion in the vicinity of the conserved leucine, has recently been discussed on the basis of molecular dynamics simulations (*53*, *54*).

Solid-state ^{15}N NMR data suggested a predominantly transmembrane orientation of TM2e based on the orientations of the NH bond vectors in seven leucine residues. Earlier, a transmembrane orientation of TM2 of the muscle nAChR δ subunit was also demonstrated by solid-state NMR; in addition, the orientational constraints derived from the more precise ^{1}H$-^{15}$N dipolar coupling measurements on the uniformly labeled peptide have shown that its long helix axis is tilted 12° from the lipid bilayer normal (*7*). These results, as well as the substituted cysteine accessibility data for the mouse muscle nAChR α_1 subunit (*2*), have suggested that the helical region in the TM2 domain of the membrane-bound muscle nAChR is located between the N-terminus and position 22 (glutamine in the δ subunit and glutamic acid in the α_1 subunit), which is very similar to our findings for the neuronal nAChR β_2 subunit in DPC micelles.

The dynamical properties determined in this study are in agreement with the presence of a well-defined secondary structure. High NOE and S^2 values were obtained for all seven leucine residues (Figure 5), indicating restricted internal motions of the amide bond vector for the residues in the transmembrane domain. The τ_m values are in general significantly longer in micelles than in solution because of the slower tumbling of the whole complex, including a peptide, a micelle, and a hydration layer (*47*). The τ_m value of TM2e in DPC was found to be 14.4 $\pm$ 0.2 ns, which is similar to the values typically obtained (8−20 ns) for peptides of comparable size in micelles by similar ^{15}N relaxation measurements (*55*−*59*). The experimental τ_m value is very close to 13.2 ns, a value expected for 28-residue TM2e in DPC according to the molecular mass of the peptide−micelle complex (approximately 0.5 ns/kDa for isotropic tumbling). Experimental τ_m values may reflect a minor contribution of the aggregated species. Alternatively, a higher estimated τ_m value and its slight increase with spectrometer frequency might suggest possible contributions of chemical exchange or conformational averaging on micro- to millisecond time scales (*46*). However, the R_{ex} value, when calculated, was insignificant, showing that TM2e in DPC micelles is not subject to extensive conformational exchange. Relatively slow internal motions on the sub-nanosecond to nanosecond time scale also do not contribute significantly to the TM2e backbone dynamics at leucine positions. If internal motions occurred with τ_e in the range of 0.7−1.5 ns or even to 2 ns, they could be detected using conventional model-free analysis. Internal motions with longer τ_e values manifest themselves as a characteristic decrease in the apparent τ_m, derived from the R_2/R_1 ratio, at a higher resonance frequency (*46*). No such decrease in τ_m at 600 MHz was observed, and most of the relaxation data were best described by the dynamical models without the inclusion of the τ_e parameter. The absence of significant complicating effects on the peptide dynamics manifested itself in the similarity of optimized τ_m values to those estimated from the R_2/R_1 ratio (14.4 and 15.2 ns at 401 and 600 MHz, respectively).

In the absence of published data on the dynamics of transmembrane nAChR peptides, the findings presented here for TM2e can be compared with results of the studies of other membrane proteins in micelles. In earlier studies of bacteriophage coat proteins in SDS, the presence of two membrane-associated helices with different motional characteristics has been demonstrated (*55*, *56*). Typical R_2, NOE, and S^2 values for the helical region of TM2e given here in Figure 5 were almost identical to the values reported for the hydrophobic helix but not to those of the amphipathic helix in the coat proteins. Notably, the hydrophobic helix penetrates the micelle interior, contrary to the amphipathic helix located on the micelle surface (*55*, *56*). This comparison supports the characterization of the nAChR TM2e as a transmembrane peptide. TM2e exhibited significantly higher backbone rigidity than the uniformly ^{15}N-labeled TM2 peptide of the neuronal GlyR α_1 subunit, which also adopted helical structure in DPC and SDS micelles (*8*, *9*). In contrast with the TM2 domain of the GlyR α_1 subunit in SDS micelles, where the data led us to assume the possibility of internal motions on the sub-nanosecond to nanosecond time scale (*9*), no evidence for such motions was found for β_2 TM2e of the nAChR.

This work appears to be a first glance at the structure and backbone dynamics of the TM2 domain of the human nAChR β_2 subunit in membrane-mimetic environment. Seven [^{15}N]Leu labels are evenly distributed along the TM2e chain, thus adequately reflecting the dynamics of TM2e as a whole. Although the structure and dynamics were studied for the relatively short and isolated transmembrane peptide, these results could be related to the important general characteristics of the whole nAChR helical bundle, because even the isolated nAChR TM2 segments are able to form functional channels in bilayers (*7*). However, caution should be exercised in extrapolating any particular details to the intact receptors, because they may depend on the selection of the domain boundaries for subcloning the isolated protein fragments, and on the micelle properties (*9*). Nevertheless, our findings provide a necessary scaffold for subsequent studies of nAChR interactions with small ligands, such as general anesthetics.

ACKNOWLEDGMENT

We thank Dr. Dejian Ma and Dr. Pravat Mandal for acquiring spectra on the Avance-600 spectrometer and Ms. Martha Zegarra and Ms. Ling Li for technical support. We also thank Prof. Tim Cross, Mr. Yiming Mo, and Dr. Riqiang Fu (CIMAR/NHMFL, Tallahassee, FL) for the solid-state ^{15}N NMR measurements.

SUPPORTING INFORMATION AVAILABLE

^{1}H and ^{15}N peak assignments for TM2e in DPC micelles. This material is available free of charge via the Internet at http://pubs.acs.org.

REFERENCES

1. Bock, G., and Goode, J. (2002) in *Novartis Foundation Symposium*, Vol. 273, 245 pp, Wiley, Chichester, U.K.
2. Karlin, A. (2002) *Nat. Rev. Neurosci. 3*, 102−114.
3. Hucho, F., Tsetlin, V. I., and Machold, J. (1996) *Eur. J. Biochem. 239*, 539−557.
4. Unwin, N. (1995) *Nature 373*, 37−43.
5. Miyazawa, A., Fujiyoshi, Y., and Unwin, N. (2003) *Nature 424*, 949−955.

6. Brejc, K., van Dijk, W. J., Klaassen, R. V., Schuurmans, M., van der Oost, J., Smit, A. B., and Sixma, T. K. (2001) *Nature 411*, 269−276.
7. Opella, S. J., Marassi, F. M., Gesell, J. J., Valente, A. P., Kim, Y., Oblatt-Montal, M., and Montal, M. (1999) *Nat. Struct. Biol. 6*, 374−379.
8. Tang, P., Mandal, P. K., and Xu, Y. (2002) *Biophys. J. 83*, 252−262.
9. Yushmanov, V. E., Mandal, P. K., Liu, Z., Tang, P., and Xu, Y. (2003) *Biochemistry 42*, 3989−3995.
10. Lugovskoy, A. A., Maslennikov, I. V., Utkin, Y. N., Tsetlin, V. I., Cohen, J. B., and Arseniev, A. S. (1998) *Eur. J. Biochem. 255*, 455−461.
11. Pashkov, V. S., Maslennikov, I. V., Tchikin, L. D., Efremov, R. G., Ivanov, V. T., and Arseniev, A. S. (1999) *FEBS Lett. 457*, 117−121.
12. Opella, S. J., Gesell, J., Valente, A. P., Marassi, F. M., Oblatt-Montal, M., Sun, W., Ferrer-Montiel, A., and Montal, M. (1997) *Chemtracts: Biochem. Mol. Biol. 10*, 153−174.
13. McGehee, D. S. (1999) *Ann. N.Y. Acad. Sci. 868*, 565−577.
14. Hogg, R. C., Raggenbass, M., and Bertrand, D. (2003) *Rev. Physiol. Biochem. Pharmacol. 147*, 1−46.
15. Rossi, F. M., Pizzorusso, T., Porciatti, V., Marubio, L. M., Maffei, L., and Changeux, J. P. (2001) *Proc. Natl. Acad. Sci. U.S.A. 98*, 6453−6458.
16. Cohen, G., Han, Z. Y., Grailhe, R., Gallego, J., Gaultier, C., Changeux, J. P., and Lagercrantz, H. (2002) *Proc. Natl. Acad. Sci. U.S.A. 99*, 13272−13277.
17. Engidawork, E., Gulesserian, T., Balic, N., Cairns, N., and Lubec, G. (2001) *J. Neural Transm., Suppl.*, 211−222.
18. De Fusco, M., Becchetti, A., Patrignani, A., Annesi, G., Gambardella, A., Quattrone, A., Ballabio, A., Wanke, E., and Casari, G. (2000) *Nat. Genet. 26*, 275−276.
19. Flood, P., Ramirez-Latorre, J., and Role, L. (1997) *Anesthesiology 86*, 859−865.
20. Violet, J. M., Downie, D. L., Nakisa, R. C., Lieb, W. R., and Franks, N. P. (1997) *Anesthesiology 86*, 866−874.
21. Yamakura, T., Borghese, C., and Harris, R. A. (2000) *J. Biol. Chem. 275*, 40879−40886.
22. Forman, S. A., Miller, K. W., and Yellen, G. (1995) *Mol. Pharmacol. 48*, 574−581.
23. Kay, L. E. (1998) *Nat. Struct. Biol. 5* (Suppl.), 513−517.
24. Tang, P., and Xu, Y. (2002) *Proc. Natl. Acad. Sci. U.S.A. 99*, 16035−16040.
25. Tang, P., Mandal, P. K., and Zegarra, M. (2002) *Biophys. J. 83*, 1413−1420.
26. Palmer, A. G., III (2001) *Annu. Rev. Biophys. Biomol. Struct. 30*, 129−155.
27. Tian, C. L., Tobler, K., Lamb, R. A., Pinto, L. H., and Cross, T. A. (2002) *Biochemistry 41*, 11294−11300.
28. Lobley, A., Whitmore, L., and Wallace, B. A. (2002) *Bioinformatics 18*, 211−212.
29. Farrow, N. A., Muhandiram, R., Singer, A. U., Pascal, S. M., Kay, C. M., Gish, G., Shoelson, S. E., Pawson, T., Forman-Kay, J. D., and Kay, L. E. (1994) *Biochemistry 33*, 5984−6003.
30. Delaglio, F., Grzesiek, S., Vuister, G. W., Zhu, G., Pfeifer, J., and Bax, A. (1995) *J. Biomol. NMR 6*, 277−293.
31. Garrett, D. S., Powers, R., Gronenborn, A. M., and Clore, G. M. (1991) *J. Magn. Reson. 95*, 214−220.
32. Goddard, T. D., and Kneller, D. G. (2001) *SPARKY 3*, University of California, San Francisco.
33. Cai, M., Huang, Y., Zheng, R., Wei, S. Q., Ghirlando, R., Lee, M. S., Craigie, R., Gronenborn, A. M., and Clore, G. M. (1998) *Nat. Struct. Biol. 5*, 903−909.
34. Baker, E. N., and Hubbard, R. E. (1984) *Prog. Biophys. Mol. Biol. 44*, 97−179.
35. Mitchell, J. B. O., and Price, S. L. (1990) *J. Comput. Chem. 11*, 1217−1233.
36. Nilges, M., Clore, G. M., and Gronenborn, A. M. (1988) *FEBS Lett. 229*, 317−324.
37. Brünger, A. T. (1992) *X-PLOR: A system for X-ray crystallography and NMR*, version 3.581, Yale University Press, New Haven, CT.
38. Clore, G. M., and Gronenborn, A. M. (1998) *Proc. Natl. Acad. Sci. U.S.A. 95*, 5891−5898.
39. Kay, L. E., Torchia, D. A., and Bax, A. (1989) *Biochemistry 28*, 8972−8979.
40. Dosset, P., Hus, J.-C., Blackledge, M., and Marion, D. (2000) *J. Biomol. NMR 16*, 23−28.
41. Lipari, G., and Szabo, A. (1982) *J. Am. Chem. Soc. 104*, 4546−4559.
42. Lipari, G., and Szabo, A. (1982) *J. Am. Chem. Soc. 104*, 4559−4570.
43. Palmer, A. G., III, Rance, M., and Wright, P. E. (1991) *J. Am. Chem. Soc. 113*, 4371−4380.
44. Mandel, A. M., Akke, M., and Palmer, A. G., III (1995) *J. Mol. Biol. 246*, 144−163.
45. Wishart, D. S., Sykes, B. D., and Richards, F. M. (1992) *Biochemistry 31*, 1647−1651.
46. Orekhov, V. Y., Korzhnev, D. M., Pervushin, K. V., Hoffmann, E., and Arseniev, A. S. (1999) *J. Biomol. Struct. Dyn. 17*, 157−174.
47. Damberg, P., Jarvet, J., and Graslund, A. (2001) *Methods Enzymol. 339*, 271−285.
48. Papavoine, C. H., Konings, R. N., Hilbers, C. W., and van de Ven, F. J. (1994) *Biochemistry 33*, 12990−12997.
49. Yushmanov, V. E., Imasato, H., Perussi, J. R., and Tabak, M. (1995) *J. Magn. Reson., Ser. B 106*, 236−244.
50. Almeida, L. E., Borissevitch, I. E., Yushmanov, V. E., and Tabak, M. (1998) *J. Colloid Interface Sci. 203*, 456−463.
51. Wienk, H. L., Wechselberger, R. W., Czisch, M., and de Kruijff, B. (2000) *Biochemistry 39*, 8219−8227.
52. Brown, L. R., Bosch, C., and Wuthrich, K. (1981) *Biochim. Biophys. Acta 642*, 296−312.
53. Bertaccini, E., and Trudell, J. R. (2002) *Protein Eng. 15*, 443−454.
54. Sansom, M. S., Adcock, C., and Smith, G. R. (1998) *J. Struct. Biol. 121*, 246−262.
55. Almeida, F. C., and Opella, S. J. (1997) *J. Mol. Biol. 270*, 481−495.
56. Papavoine, C. H., Remerowski, M. L., Horstink, L. M., Konings, R. N., Hilbers, C. W., and van de Ven, F. J. (1997) *Biochemistry 36*, 4015−4026.
57. Williams, K. A., Farrow, N. A., Deber, C. M., and Kay, L. E. (1996) *Biochemistry 35*, 5145−5157.
58. Yan, C., Digate, R. J., and Guiles, R. D. (1999) *Biopolymers 49*, 55−70.
59. Sorgen, P. L., Cahill, S. M., Krueger-Koplin, R. D., Krueger-Koplin, S. T., Schenck, C. C., and Girvin, M. E. (2002) *Biochemistry 41*, 31−41.

BI0350396